Nanoscale

RSC Publishing

PAPER

View Article Online
View Journal | View Issue

Published on 26 November 2012. Downloaded by University of Prince Edward Island on 30/10/2014 21:52:29.

Cite this: *Nanoscale*, 2013, **5**, 1121

The vital function of Fe_3O_4@Au nanocomposites for hydrolase biosensor design and its application in detection of methyl parathion†

Yuting Zhao,[a] Weiying Zhang,[b] Yuehe Lin[b] and Dan Du*[a]

A nanocomposite of gold nanoparticles (AuNPs) decorating a magnetic Fe_3O_4 core was synthesized using cysteamine (SH–NH_2) as linker, and characterized by TEM, XPS, UV and electrochemistry. Then a hydrolase biosensor, based on self-assembly of methyl parathion hydrolase (MPH) on the Fe_3O_4@Au nanocomposite, was developed for sensitive and selective detection of the organophosphorus pesticide (OP) methyl parathion. The magnetic nanocomposite provides an easy way to construct the enzyme biosensor by simply exerting an external magnetic field, and also provides a simple way to renew the electrode surface by removing the magnet. Unlike inhibition-based enzyme biosensors, the hydrolase is not poisoned by OPs and thus is reusable for continuous measurement. AuNPs not only provide a large surface area, high loading efficiency and fast electron transfer, but also stabilize the enzyme through electrostatic interactions. The MPH biosensor shows rapid response and high selectivity for detection of methyl parathion, with a linear range from 0.5 to 1000 ng mL^{-1} and a detection limit of 0.1 ng mL^{-1}. It also shows acceptable reproducibility and stability. The simplicity and ease of operation of the proposed method has great potential for on-site detection of P–S containing pesticides and provides a promising strategy to construct a robust biosensor.

Received 9th October 2012
Accepted 21st November 2012

DOI: 10.1039/c2nr33107a

www.rsc.org/nanoscale

Introduction

Organophosphorus (OP) compounds have been widely used as pesticides, and some have been developed as chemical nerve agents, such as soman, sarin, tabun, VX (*O*-ethyl *S*-diisopropylaminomethyl methylphosphonothiolate) and others.[1,2] They exert their toxicity through irreversible phosphorylation and inactivation of acetylcholinesterase (AChE) in the central nervous system, often leading to perturbation of the nerve conduction system and to the rapid paralysis of vital functions of living systems.[3,4] Although liquid or gas chromatography coupled with mass spectrometry (LC/GC-MS) is generally performed for detection of OP compounds with good sensitivity and accuracy,[5,6] they are very expensive, time-consuming and laboratory-oriented methods. Enzyme based electrochemical biosensors are excellent candidates in low-cost and field-deployable detection due to their rapid response, ease of operation and small size. Several enzymes, such as AChE, ascorbate oxidase, and tyrosinase have been applied in biosensors for the detection of target analytes.[7–9] Among these, AChE biosensors are most attractive.[10–12] However, such inhibition biosensors are not specific to OPs, since AChE is also the target of carbamate pesticides. Differing from AChE, the organophosphorus hydrolase (OPH) biosensor is based on the hydrolysis of OPs to produce less toxic electroactive products such as *p*-nitrophenol (PNP) and diethyl phosphate.[13] This process is reversible and the obtained signal is positively proportional to the amount of OPs.[14]

For fabrication of stable and sensitive biosensors, the strategy for immobilization of the enzyme onto the electrode surface is one of the most important factors. Most reported methods such as physical adsorption and entrapment can maintain the activity of the immobilized enzyme but may cause leakage from the electrode surface; covalent binding gives a firm immobilization of the enzyme but tends to partially denature its activity.[15] Electrostatic adsorption, combining the advantages of both physical adsorption and covalent binding, is a good method for biosensor design.[16] The sensitivity of the biosensor can be further enhanced by using various nanomaterial-based amplifications. Au nanoparticles (AuNPs) have shown remarkable advantages including high conductivity, high catalytic efficiency, excellent biocompatibility and little cytotoxicity even *in vivo*. They are also easily functionalized to immobilize biomolecules.[17–21] Core–shell-structured magnetic Fe_3O_4@Au nanocomposites have attracted enormous interest in bio-assays. For example, Sun *et al.*[22,23] successfully prepared dumbbell-like Fe_3O_4@Au nanoparticles which show excellent

[a]*Key Laboratory of Pesticide and Chemical Biology of Ministry of Education, College of Chemistry, Central China Normal University, Wuhan 430079, PR China. E-mail: dudan@mail.ccnu.edu.cn; Fax: +86 27 67867953; Tel: +86 27 67867958*

[b]*Pacific Northwest National Laboratory, Richland, WA 99352, USA*

† Electronic supplementary information (ESI) available. See DOI: 10.1039/c2nr33107a

This journal is © The Royal Society of Chemistry 2013

Published on 26 November 2012. Downloaded by University of Prince Edward Island on 30/10/2014 21:52:29.

optical and magnetic properties and can act as target-specific nanocarriers to deliver platin into Her2-positive breast cancer cells with strong therapeutic effects. Li's group[24] synthesized bifunctional Fe_3O_4@Au nanoparticles for separating proteins. Chen *et al.*[25] reported the preparation of a Fe_3O_4–Ppy–Au nanocomposite which exhibits excellent electrocatalytic activity to ascorbic acid. Our group also developed a novel oxidative desorption of thiocholine assembled on core–shell Fe_3O_4@Au magnetic nanocomposites for determination of AChE activity in human serum.[26]

Here, we reported a strategy of decorating AuNPs on the Fe_3O_4 core using cysteamine (SH–NH_2) as a linker. We further fabricated an electrochemical biosensor based on self-assembling one member of the OPH family, methyl parathion hydrolase (MPH), onto core–shell-structured Fe_3O_4@Au nanocomposites. Positively charged MPH (pI 8.3) is quickly and strongly adsorbed onto the negatively charged Fe_3O_4@Au nanocomposite. Self-assembly is easy and fast to realize through electrostatic interaction. We are also aiming to look at the vital function of AuNPs for biosensor design and its application for the detection of OP pesticides (Scheme 1).

Experimental methods

1 Reagents

Methyl parathion, cysteamine, *N*-hydroxysuccinimide (NHS), 1-ethyl-3-(3-dimethylaminopropyl) carbodiimide hydrochloride (EDC) and phosphate buffer saline (PBS) were purchased from Sigma-Aldrich Co. (St. Louis, USA). Chloroauric acid ($AuCl_3 \cdot HCl \cdot 4H_2O$, Au 47.8%) was obtained from Sinopharm Chemical Reagent Co. Ltd (Shanghai, China). Carboxylated Fe_3O_4 was purchased from Tianjin Baseline ChromTech Research Centre (Tianjin, China). Trisodium citrate, $NaBH_4$ and other reagents used were analytical reagent grade and obtained from Shanghai Chemical Reagent Co. (Shanghai, China). Methyl parathion hydrolase (MPH) was isolated and purified by Prof. Deli Liu's lab.[27]

2 Synthesis of Fe_3O_4@Au magnetic nanocomposites

AuNPs with average diameter of 13 nm were synthesized according to the citrate reduction of $HAuCl_4$.[28] The method is briefly depicted as follows: A 100 mL aqueous solution of 0.01% $HAuCl_4$ was heated to boiling and vigorously stirred in a 250 mL round-bottom flask; rapid addition of 2 mL of 1% trisodium citrate to the solution resulted in a colour change from pale yellow to wine-red after 60 s. Boiling was continued for an additional 10 min, then the heating mantle was removed, and the solution kept stirring for another 15 min. The colloids were stored in dark bottles at 4 °C. Different sizes of AuNPs were obtained by varying the ratio of $HAuCl_4$ to trisodium citrate.

The purified carboxylated Fe_3O_4 nanoparticles were firstly functionalized with SH–NH_2. Briefly, 2.0 mL carboxylated Fe_3O_4 (1.0 mg mL^{-1}) was mixed with 400 mM EDC and 100 mM NHS for a reaction time of 1 h. The reactivated Fe_3O_4 was separated by using a magnet at the bottom of the tube and washed with double-distilled water three times to remove excess EDC and NHS. It was re-dispersed in 4.0 mL SH–NH_2 solution (50 mM) and kept for 3 h, then magnetically separated and washed with double-distilled water to remove excess SH–NH_2. After that, 10 mL synthesized AuNPs solution was mixed with the SH–NH_2/Fe_3O_4 collection and kept stirring for another 3 h. The resulting Fe_3O_4@Au nanocomposite was separated and washed three times with double-distilled water. It was re-dispersed in 4.0 mL PBS and kept at 4 °C for the following experiment.

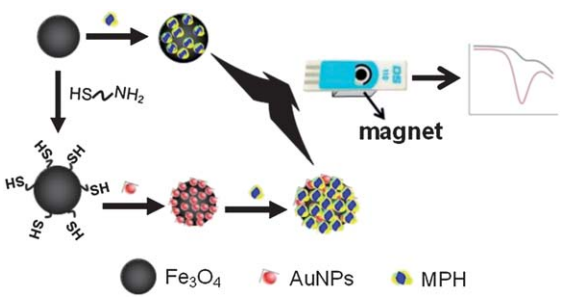

Scheme 1 Preparation of Fe_3O_4@Au nanocomposite or Fe_3O_4 based MPH biosensor (MPH-Fe_3O_4@Au/SPE, MPH-Fe_3O_4/SPE) and its application for detection of methyl parathion.

3 Fabrication of biosensor

4.0 mL Fe_3O_4@Au was dispersed into 4.0 mL MPH solution for incubation overnight. The resulting MPH-Fe_3O_4@Au nanocomposites were washed and separated by magnetic steps, and re-dispersed in 4.0 mL pH 7.4 PBS. For comparison, MPH-Fe_3O_4 was prepared by directly mixing the EDC-NHS activated Fe_3O_4 with MPH solution. After that, a volume of 10 μL MPH-Fe_3O_4@Au or MPH-Fe_3O_4 was pipetted onto the working area of the screen printed electrode (SPE) with a magnet beneath it.

4 Characterization and electrochemical measurements

Transmission electron microscopy (TEM) micrographs were performed on a JEOL 2000 transmission electron microscope operating at 200 kV. UV spectra were recorded using a UV-2501 spectrophotometer (Shimadzu, Japan). X-ray photoelectron spectroscopy (XPS) measurements were carried out with a Thermo Electron instrument MultiLab 2000 (Thermo Fisher, USA). Electrochemical measurements were performed on a CHI 660C workstation (CH Instruments Co., Shanghai, China). A disposable SPE consisting of a carbon working electrode, a carbon counter electrode, and an Ag/AgCl reference electrode were purchased from DropSens (Oviedo, Spain).

Results and discussion

1 Characterization of Fe_3O_4@Au magnetic nanocomposites

Fig. 1A shows photographs taken during the synthetic procedure. The colloidal AuNPs solution is stable and displays a typical red color (a). After adding SH–NH_2 functionalized Fe_3O_4 (b) and ultrasonication (c), a homogeneous and dark purple suspension was achieved. The resulted Fe_3O_4@Au magnetic nanocomposites were easily and quickly separated by using an external magnet, leaving a clear and transparent bulk solution (d). This result demonstrated that AuNPs were successfully

 This journal is © The Royal Society of Chemistry 2013

Published on 26 November 2012. Downloaded by University of Prince Edward Island on 30/10/2014 21:52:29.

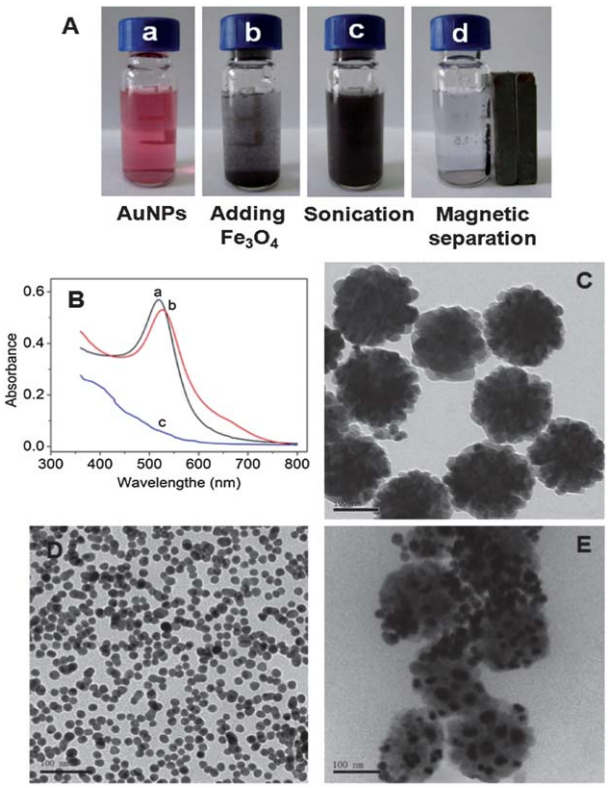

Fig. 1 (A) Photographs taken during the synthesis of Fe_3O_4@Au nanocomposites. (B) The UV-vis absorption spectra of colloidal AuNPs (a), Fe_3O_4@Au nanocomposites suspension (b) and the supernatant after magnetic separation (c). (C) TEM images of Fe_3O_4, (D) AuNPs and (E) Fe_3O_4@Au nanocomposites.

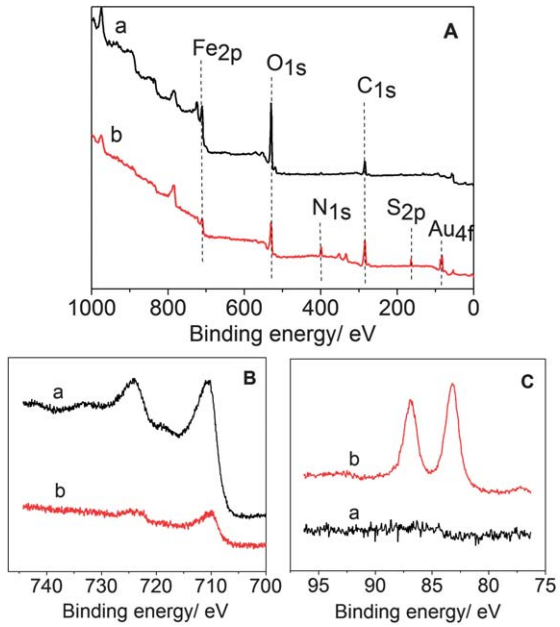

Fig. 2 (A) XPS spectra of Fe_3O_4 (a) and Fe_3O_4@Au nanocomposites (b), (B) Fe_{2p} of Fe_3O_4 (a) and Fe_3O_4@Au nanocomposites (b), (C) Au_{4f} of Fe_3O_4 (a) and Fe_3O_4@Au nanocomposites (b).

adsorbed on the Fe_3O_4 surface. When removing the magnetic force, the nanocomposites were easily re-dispersed with sonication, indicating that the magnet only attracted the nanocomposites to the corresponding position and did not cause any structural change.[29] This property allows them to be easily deposited on the SPE by applying magnetic force.

The UV-vis absorption spectra of colloidal AuNPs (curve a), Fe_3O_4@Au nanocomposites suspension (curve b) and the supernatant after magnetic separation (curve c) were further shown in Fig. 1B. Both of them display an absorption peak at 518 nm and 528 nm, respectively, which is the characteristic band of well-dispersed AuNPs. The small red-shift might result from the interaction between AuNPs and Fe_3O_4. From the loss of intensity, we make a rough estimation that more than 95% of AuNPs have been loaded on the Fe_3O_4. After magnetic separation the supernatant did not show measurable absorbance, which further indicates that AuNPs are effectively adsorbed on the Fe_3O_4.

Fig. 1C–E show the typical TEM images of Fe_3O_4 (C), AuNPs (D) and Fe_3O_4@Au nanocomposites (E). A uniform spherical morphology of Fe_3O_4 was observed with an average diameter of 120 nm. The AuNPs were clearly identifiable and appeared uniform in size with a diameter of ~13 nm. As shown in Fig. 2E, the synthesized Fe_3O_4@Au nanocomposites were clearly observed and the AuNPs were scattered uniformly on the Fe_3O_4.

XPS was further employed to compare the two interfaces of Fe_3O_4 and Fe_3O_4@Au nanocomposites. As shown in the full spectra of Fig. 2A, both Fe_3O_4 (curve a) and Fe_3O_4@Au nanocomposites (curve b) present distinct peaks at 726.5 eV, 710.3 eV and 528.9 eV, which are attributed to $Fe2p_{1/2}$, $Fe2p_{3/2}$ and O^{2-} of the O1s, respectively. New peaks at 397.6 eV and 163.3 eV appeared in curve b. They are the positions of N1s and S2p, indicating the introduction of SH–NH_2 during the synthesis of Fe_3O_4@Au nanocomposites. The peak doublet appearing at 83.7 eV ($Au4f_{7/2}$) and 86.9 eV ($Au4f_{5/2}$) is assigned to Au^0. This conclusion was also supported by high-resolution XPS spectra of Fe2p and Au4f, as shown in Fig. 2B and C. The groups at 726.5 eV and 710.3 eV correspond to $Fe2p_{1/2}$ and $Fe2p_{3/2}$, respectively. It can be seen that the intensity in curve b decreases compared with curve a. In Fig. 2C, two peaks of Au $4f_{5/2}$ and Au $4f_{7/2}$ are clearly observed in Fe_3O_4@Au nanocomposites (curve b) while no peaks in Fe_3O_4 (curve a) are seen.

2 Function of AuNPs for biosensor design

To understand the function of AuNPs in biosensing, we compared photometric and electrocatalytic responses of MPH/Fe_3O_4 and MPH/Fe_3O_4@Au. It is known that MPH catalyzes the hydrolysis of methyl parathion (λ_{max} = 274 nm) to release an equimolar amount of PNP (λ_{max} = 405 nm).[30] Thus, UV-vis spectroscopy can be used to measure the enzymatic product of OP. As shown in Fig. 3A, the peak at 274 nm decreased greatly after the MPH/Fe_3O_4 (curve b) and MPH/Fe_3O_4@Au (curve c) were exposed to 100 ng mL^{-1} methyl parathion for 10 min compared to the control of pre-exposure, *i.e.* methyl parathion solution (curve a). A new peak appeared at 405 nm corresponding to PNP. The decrease in methyl parathion absorption at 274 nm is paralleled by an increase in PNP absorption at 400 nm, which indicates that MPH/Fe_3O_4@Au has a higher hydrolysis activity than MPH/Fe_3O_4.

Published on 26 November 2012. Downloaded by University of Prince Edward Island on 30/10/2014 21:52:29.

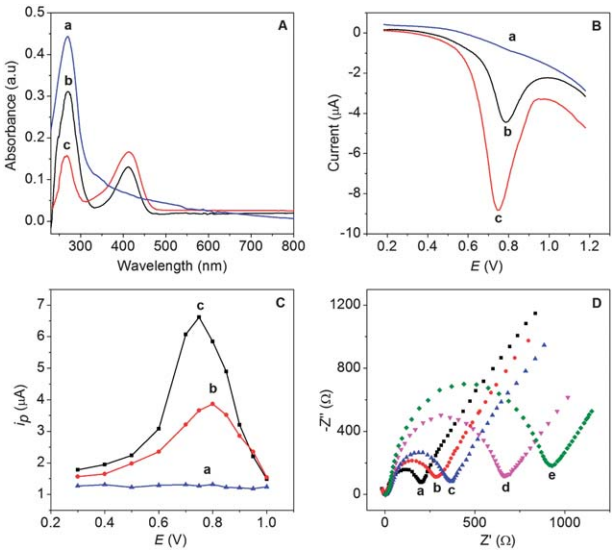

Fig. 3 (A) UV-vis spectroscopy of 100 ng mL^{-1} methyl parathion solution (a), after exposure of MPH/Fe_3O_4 (b) and MPH/Fe_3O_4@Au (c) to 100 ng mL^{-1} methyl parathion for 10 min, respectively. (B) SWV measurements of MPH/Fe_3O_4@Au/SPE in pH 7.4 PBS in the absence of methyl parathion (a), MPH/Fe_3O_4/SPE (b) and MPH/Fe_3O_4@Au/SPE (c) in pH 7.4 PBS in the presence of 100 ng mL^{-1} methyl parathion. (C) Hydrodynamic voltammograms of 100 ng mL^{-1} methyl parathion at bare SPE (a), MPH/Fe_3O_4/SPE (b) and MPH/Fe_3O_4@Au/SPE (c). (D) EIS measurements at bare SPE (a), Fe_3O_4@Au/SPE (b), Fe_3O_4/SPE (c), MPH-Fe_3O_4@Au/SPE (d) and MPH-Fe_3O_4/SPE (e). The electrochemical impedance experiment was carried out in 10 mM $Fe(CN)_6^{4-/3-}$ with frequencies ranging from 100 kHz to 0.1 Hz with an amplitude of 5 mV.

The hydrolysis product, PNP, is also electroactive and can be oxidized to generate measurable current which is related to the concentration of methyl parathion. As shown by square wave voltammetry (SWV) in Fig. 3B, no peak was observed at MPH/Fe_3O_4@Au/SPE (curve a) in pH 7.4 PBS in the absence of methyl parathion. After adding 100 ng mL^{-1} methyl parathion to the PBS, a well-defined oxidative peak appeared for both MPH/Fe_3O_4/SPE (curve b) and MPH/Fe_3O_4@Au/SPE (curve c). Obviously, this peak arose from the oxidation of PNP, which is the hydrolysis product of methyl parathion. Furthermore, the peak current on MPH/Fe_3O_4@Au/SPE was 2-fold higher and the peak potential shifted 70 mV negatively compared to those on MPH/Fe_3O_4/SPE. This was because of the presence of AuNPs, with their inherent conductive properties and high catalytic behaviour, which provides a conductive pathway for electron transfer and promotes electron-transfer at a lower potential.

The data from hydrodynamic voltammograms also confirmed the results in SWV measurements. It can be seen from Fig. 3C that methyl parathion (100 ng mL^{-1}) did not show measurable response on the bare SPE (curve a). The current response started at 0.6 V and increased to a maximum at ~0.80 V and ~0.75 V on MPH/Fe_3O_4/SPE (curve b) and MPH/Fe_3O_4@Au/SPE (curve c), respectively. The AuNPs-containing MPH electrode displayed a higher current than the "AuNPs-free" biosensor, indicating that AuNPs play an important role in electron transfer.

EIS was further performed to give information on electron-transfer kinetics at the electrode surface. As shown in Fig. 3D, a small resistance was exhibited on the bare SPE (curve a). After the electrode was treated with Fe_3O_4@Au, the EIS increased slightly (curve b). If Fe_3O_4 was directly coated on the SPE, a much higher resistance was observed (curve c). Further introducing MPH to the Fe_3O_4@Au modified electrode surface led to a significant increase of resistance (curve d) because the protein layer insulates the conductive support and perturbs interfacial electron-transfer, which also confirmed the immobilization of MPH on the electrode surface. While if MPH was coated on the Fe_3O_4/SPE without AuNPs, the resistance continued increasing (curve e). This result also confirmed the high electronic conductivity of AuNPs.[31]

3 Optimization of the nanocomposites preparation

The amount of AuNPs plays an important role in the sensitivity of the biosensor. As shown in Fig. 4A, the current response increased with increasing AuNP content in the nanocomposites due to an increased conductivity and reached a maximum at the volumetric ratio of 5 (AuNPs/Fe_3O_4). Further increasing the amount of AuNPs led to a decrease in response, possibly because the conglomerate of nanoparticles increases the interfacial resistance, as reported in other amperometric biosensors.[32]

The size of AuNPs is another factor affecting the signal. Fig. 4B showed the current responses of the biosensor with different sizes of AuNPs from 8 nm to 50 nm. The maximum response was obtained at 8–13 nm AuNPs. Small-sized AuNPs have an increased density on the Fe_3O_4 surface and provide more active binding sites for immobilization of MPH, thus exhibit the largest response. Since 8 nm AuNPs are not very stable and occasionally accumulate easily, 13 nm AuNPs were used in the experiment.

4 Analytical performance

Under the optimized conditions, the MPH/Fe_3O_4@Au/SPE was used for detection of methyl parathion. As shown in Fig. 5A, the current increased with the increase of pesticide concentration. It is proportional to methyl parathion concentrations in the range of 0.5–1000 ng mL^{-1} (curve a, Fig. 5B), with the detection limit of 0.1 ng mL^{-1}. For comparison, MPH/Fe_3O_4/SPE was also used for methyl parathion detection. As expected it showed much lower sensitivity and a narrow linear range (curve b, Fig. 5B).

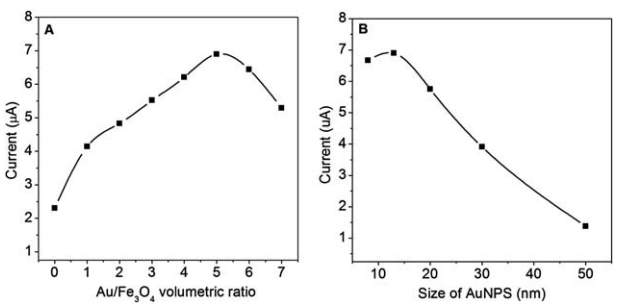

Fig. 4 Effect of the amount of AuNPs (A) and the size of AuNPs (B) on the response.

This journal is © The Royal Society of Chemistry 2013

Published on 26 November 2012. Downloaded by University of Prince Edward Island on 30/10/2014 21:52:29.

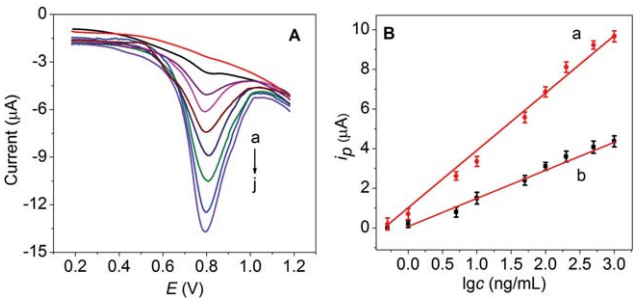

Fig. 5 (A) SWV measurements of methyl parathion with different concentrations of 0.5 (a), 1.0 (b), 5.0 (c), 10 (d), 50 (e), 100 (f), 200 (g), 500 (h), 1000 ng mL^{-1} (i). (B) Calibration curves obtained at MPH/Fe_3O_4@Au/SPE (a) and MPH/Fe_3O_4/SPE (b). Analysis parameters of SWV measurements include the applied potential range of 0.1 V to 1.2 V, a step potential of 4 mV, an amplitude of 25 mV, and a frequency of 15 Hz.

Interferences arising from carbamate pesticides, other OP pesticides such as dimethoate, monocrotophos and malathion, and oxygen-containing inorganic ions (SO_4^{2-}, NO_3^-) were further detected (ESI, Fig. S1†). They do not interfere with the detection of methyl parathion due to the high selectivity of MPH to P–S containing pesticides.

Since MPH is not poisoned by OP pesticides, unlike AChE, the MPH-biosensor is reusable and suitable for continuous measurement. The intra-assay precision was evaluated by assaying one enzyme electrode for six replicate determinations in 100 ng mL^{-1} methyl parathion and the relative standard deviation (RSD) was 4.6%. Similarly, the inter-assay precision, *i.e.* fabrication reproducibility, was estimated at six different electrodes and the RSD was 7.8%. These results indicated acceptable precision and reproducibility. When the enzyme electrode was not in use, it was stored at 4 °C under dry conditions. No obvious decrease in response was observed in the first 7 days of storage. After a 30 day storage period, the sensor retained 80% of its initial current response, indicating acceptable stability (ESI, Fig. S2†).

Conclusions

In summary, we have reported a sensitive and selective hydrolase biosensor based on self-assembly of MPH for detecting methyl parathion and demonstrated the particular function of AuNPs in biosensing. Several advantages of the proposed method should be highlighted. First, due to the high electronic conductivity, high catalytic efficiency, large surface area and excellent biocompatibility of AuNPs, the constructed MPH biosensor presents a fast and sensitive response. Second, the electrostatic interaction between positively charged MPH and negatively charged AuNPs prevents the enzyme from aggregating on the Fe_3O_4 core and enhances the stability of the immobilized enzyme. Third, the magnetic nanocomposite provides an easy way to construct an enzyme biosensor by simply exerting an external magnetic field, and also provides a simple way to renew the electrode surface by removing the magnet. Fourth, the high selectivity of MPH towards P–S containing pesticides precludes other possible interference. This nanoassembly protocol is expected to be used for immobilization of various enzymes and proteins, leading to robust biosensors.

Acknowledgements

This work was supported by the National Natural Science Foundation of China (21275062, 21075047) and the self-determined research funds of CCNU from the colleges' basic research and operation of MOE (CCNU11C01002). Y. Lin acknowledges the financial support by the CounterACT Program, Office of the Director, National Institutes of Health (OD) and the National Institute of Neurological Disorders and Stroke (NINDS), grant number U01 NS058161-01. The contents of this publication are solely the responsibility of the authors and do not necessarily represent the official views of the NIH. Pacific Northwest National Laboratory is operated by Battelle for US-DOE under Contract DE-AC05-76RL01830. We specially thank Prof. Deli Liu in Central China Normal University for providing MPH.

Notes and references

1 B. C. Giordano and G. E. Collins, *Curr. Org. Chem.*, 2007, **11**, 255–256.
2 G. D. Ding, P. Wang, Y. Tian, J. Zhang, Y. Gao, X. J. Wang, R. Shi, G. Q. Wang and X. M. Shen, *Environ. Sci. Technol.*, 2012, **46**, 2911–2917.
3 G. Mercey, T. Verdelet, J. Renou, M. Kliachyna, R. Baati, F. Nachon, L. Jean and P. Y. Renard, *Acc. Chem. Res.*, 2012, **45**, 756–766.
4 M. Eddleston, N. A. Buckley, P. Eyer and A. H. Dawson, *Lancet*, 2008, **371**, 597–607.
5 L. Rotiroti, L. D. Stefano, I. Rendina and L. Moretti, *Biosens. Bioelectron.*, 2005, **20**, 2136–2139.
6 C. C. Leandro, P. Hancock, R. J. Fussell and B. J. Keely, *J. Chromatogr., A*, 2007, **1166**, 152–162.
7 D. Du, S. Z. Chen, J. Cai and A. D. Zhang, *Biosens. Bioelectron.*, 2007, **23**, 130–134.
8 M. Trojanowicz, *Electroanalysis*, 2002, **14**, 19–20.
9 N. Kohli, D. Srivastava, J. Sun, R. J. Richardson, I. Lee and R. M. Worden, *Anal. Chem.*, 2007, **79**, 5196–5203.
10 L. Zhang, A. D. Zhang, D. Du and Y. H. Lin, *Nanoscale*, 2012, **4**, 4674–4679.
11 D. Du, S. Z. Chen, D. D. Song, H. B. Li and X. Chen, *Biosens. Bioelectron.*, 2008, **24**, 475–479.
12 D. Du, W. J. Chen, J. Cai, J. M. Zhang, H. Y. Tu and A. D. Zhang, *J. Nanosci. Nanotechnol.*, 2009, **9**, 2368–2373.
13 S. B. Bird, T. D. Sutherland, C. Gresham, J. Oakeshott, C. Scott and M. Eddleston, *Toxicology*, 2008, **247**, 88–92.
14 J. Orbulescu, A. C. Celeste, V. K. Rastogi, S. S. Saumil, J. J. DeFrank and R. M. Leblanc, *Anal. Chem.*, 2006, **78**, 7016–7021.
15 W. Zhao, P. Ge, J. J. Xu and H. Chen, *Environ. Sci. Technol.*, 2009, **43**, 6724–6729.
16 X. Wang, D. Zhou, K. Sinniah, C. Clarke, L. Birch, H. Li, T. Rayment and C. Abell, *Langmuir*, 2006, **22**, 887–892.

Published on 26 November 2012. Downloaded by University of Prince Edward Island on 30/10/2014 21:52:29.

17 J. B. Jia, B. Q. Wang, A. G. Wu, G. J. Cheng, Z. Li and S. J. Dong, *Anal. Chem.*, 2002, **74**, 2217–2223.
18 R. Shukla, V. Bansal, M. Chaudhary, A. Basu, R. R. Bhonde and M. Sastry, *Langmuir*, 2005, **21**, 10644–10654.
19 V. Pavlov, Y. Xiao, B. Shlyahovsky and I. Willner, *J. Am. Chem. Soc.*, 2004, **126**, 11768–11769.
20 M. J. Wang, C. Y. Sun, L. Y. Wang, X. H. Ji, Y. B. Bai, T. J. Li and J. H. Li, *J. Pharm. Biomed. Anal.*, 2003, **33**, 1117–1125.
21 M. J. Wang, L. Y. Wang, W. Gang, X. H. Ji, Y. B. Bai, T. J. Li, S. Y. Gong and J. H. Li, *Biosens. Bioelectron.*, 2004, **19**, 575–582.
22 C. J. Xu, B. D. Wang and S. H. Sun, *J. Am. Chem. Soc.*, 2009, **131**, 4216–4217.
23 Z. C. Xu, Y. L. Hou and S. H. Sun, *J. Am. Chem. Soc.*, 2007, **129**, 8698–8699.
24 J. Bao, W. Chen, T. T. Liu, Y. L. Zhu, P. Y. Jin, L. Y. Wang, J. F. Liu, Y. G. Wei and Y. D. Li, *ACS Nano*, 2007, **1**, 293–298.
25 H. Zhang, X. Zhong, J. J. Xu and H. Y. Chen, *Langmuir*, 2008, **24**, 13748–13752.
26 D. Du, Y. Tao, W. Y. Zhang, D. L. Liu and H. B. Li, *Biosens. Bioelectron.*, 2011, **26**, 4231–4235.
27 D. Du, W. J. Chen, W. Y. Zhang, D. L. Liu, H. B. Li and Y. H. Lin, *Biosens. Bioelectron.*, 2010, **25**, 1370–1375.
28 K. C. Grabar, R. G. Freeman, M. B. Hommer and M. J. Natan, *Anal. Chem.*, 1995, **67**, 735–743.
29 J. Tian, F. Zheng and H. Y. Zhao, *J. Phys. Chem. C*, 2011, **115**, 3304–3312.
30 D. P. Dumas, J. R. Wild and F. M. Raushel, *J. Biol. Chem.*, 1989, **264**, 19659–19665.
31 Y. J. Huang, D. Li and J. H. Li, *Chem. Phys. Lett.*, 2004, **389**, 14–18.
32 A. Mulchandani, W. Chen, P. Mulchandani, J. Wang and K. R. Rogers, *Biosens. Bioelectron.*, 2001, **16**, 225–230.

 This journal is © The Royal Society of Chemistry 2013